Journal of Applied Mechanics. Received January 08, 2019;
Accepted manuscript posted February 28, 2019. doi:10.1115/1.4043074

Fretting Wear Modeling of Cylindrical Line Contact in Plane-Strain Borne by the Finite Element Method

Huaidong Yang

and

Itzhak Green (Fellow ASME)

G. W. Woodruff School of Mechanical Engineering

Georgia Institute of Technology

Atlanta, GA 30332-0405, USA

yanghuaidong@gatech.edu and green@gatech.edu

Abstract

This is the first study to develop an empirical formulation to predict fretting wear (volume removal) under frictional conditions for plane–strain line contacts as borne out by the finite element analysis (FEA). The contact is between a deformable half-cylinder rubbing against a deformable flat block. The FEA is guided by detailed physical conceptions, with results that subsequently lead to the methodical modeling of fretting wear. The materials in contact are set first to steel/steel, then to Alloy617/Alloy617, and finally to copper/copper. Various coefficients of friction (COFs) and the Archard Wear Model are applied to the interface. Initially, pure elastic conditions are investigated. The theoretical predictions for the wear volume at the end of the partial slip condition in unidirectional sliding contact, agree very well with the FEA results. The empirical formulation for the initial gross slip distance is constructed, again revealing results that are in good agreement with those obtained from the FEA for different materials and for various scales. The Timoshenko beam theory and the tangential loading analysis of a half-elastic space are used to approximate the deflection of the half-cylinder and the flat block, respectively. That theory supports well the empirical formulation, matching closely the corresponding FEA results. The empirical formulation of the wear volume for a general cycle under fretting motion is then established. Its results are shown to be valid for different materials and various COFs when compared with the FEA results. Lastly, plasticity is introduced to the model, shown to cause two phenomena, namely junction growth and larger tangential deformations. Wear is shown to either increase or decrease depending on the combined influences of these two phenomena.

Journal of Applied Mechanics. Received January 08, 2019;
Accepted manuscript posted February 28, 2019. doi:10.1115/1.4043074

List of Figures

Journal of Applied Mechanics. Received January 08, 2019;
Accepted manuscript posted February 28, 2019. doi:10.1115/1.4043074

List of Tables

Journal of Applied Mechanics. Received January 08, 2019;
Accepted manuscript posted February 28, 2019. doi:10.1115/1.4043074

Nomenclature

A=cross section of the beam

b=half contact width

b_c=critical half contact width

C=Poisson's ratio parameter

c=stick half contact width

E=elastic modulus

E_1=elastic modulus of the half-cylinder

E_2=elastic modulus of the block

E'=equivalent elastic modulus

G=shear modulus

H=material hardness

I=second moment of area

K=dimensionless wear coefficient

L=transverse length along the cylindrical contact

M_0/L=moment on the tip of the half-cylinder per unit length

p_0=maximum contact pressure

p_{0c}=critical maximum contact pressure

P/L=normal force per unit length

P_c/L=critical normal force per unit length

P^*=normalized normal force, P/P_c

q=tangential traction, q=q'+q''

q'=tangential traction at slip region, μp(x)

q''=supplementary tangential traction at stick region

Q/L=tangential force per unit length

R=radius of half-cylinder

s=local sliding distance

s_0=local sliding distance at the initiation of the gross slip

Journal of Applied Mechanics. Received January 08, 2019;
Accepted manuscript posted February 28, 2019. doi:10.1115/1.4043074

S_n=nominal sliding distance

S_n^*= normalized nominal sliding distance, S_n/ ω_c

S_y=yield strength

$\bar{u}$=tangential displacement on the surface of a half elastic space

v=local wear volume

V=wear volume

V_0=wear volume at the initiation of the gross slip

V_c=critical wear volume

V^*= normalized wear volume, V/V_c

δ=horizontal displacement

δ^*= normalized horizontal displacement, δ/ ω_c

δ_i=initial gross slip distance

δ_{i1}=the deflection of the half-cylinder at the initiation of the gross slip

δ_{i2}=the displacement of the stick region at the initiation of the gross slip

Δ=the deflection of the half-cylinder

μ=coefficient of friction

ω=interference

ω_c=critical interference

ω^*=normalized interference, ω/ ω_c

φ=angle of the mid-surface of beam

ν_1=Poisson's ratio of the half-cylinder

ν_2=Poisson's ratio of the block

Journal of Applied Mechanics. Received January 08, 2019;
Accepted manuscript posted February 28, 2019. doi:10.1115/1.4043074

1. Introduction

Fretting is a common occurrence in engineering between two contacting bodies when an oscillatory tangential load is compounded with a normal load. It may be caused by vibration, cyclic temperature changes, cyclic loading in gears, bolts, human joints, bearings, etc. Fretting wear and fretting fatigue are two main tribological failure causes. According to Vingsbo and Söderberg [1], fretting can be sorted into stick, mixed stick-slip, and gross slip regimes. Varenberg *et al.* [2] define a slip index to determine the different fretting regimes. Under a certain normal load, the contact status goes from stick, to partial slip, and gross slip with the increase of the tangential displacement.

Experimental studies of fretting have been done thoroughly. Junction growth, i.e., the increase of the contact area, is found by Tabor [3], and by Parker and Hatch [4]. The fretting wear experiments are done in cylindrical line contacts [5], cross cylindrical contacts [6], and spherical contacts [7]. Ahmadi *et al.* conduct fretting wear experiments using an Alloy 617 ball on an Alloy flat disk [8]. An Archard wear model is used to quantify the results. Two types of wear regimes with different wear coefficients are found. One regime is running-in with a relative large wear coefficient, and the other regime is steady-state with a relative small wear coefficient.

Analytical studies on the fretting wear are relatively scarce due to the complexity arising from the frictional tangential loading. For the tangential loading of a half elastic space, there is partial slip condition according to Johnson[9]. The information about the local slip distance at the interface, in partial slip conditions, is necessary for the fretting wear analysis. The analytical solution for the local slip distance under a Hertzian pressure with a constant coefficient of friction is recorded for 3D spherical contact by Popov and Heß [10] . However, the solution for the cylindrical line contact is not available.

Numerical studies have first been done for normal contacts [11-13]. Green [14] finds theoretically the onset of plasticity in the normal contact between spherical or cylindrical bodies. The first FEA work of parallel cylindrical fretting contact is done by Gupta et al. [15]. However, their model consists of a very coarse mesh with only 285 elements, limited by the typical computational means available at that time. Recent numerical fretting analyses utilizing the FEA method with very fine meshes are done between cylindrical and spherical contacts by

Green and Yang [16-18]. The evolution of von-Mises stress, plastic strain, junction growth, fretting loop, and scars at the interface are recorded. However, these works do not apply a wear model at the interface. Ghosh et al. [19] simulate the fretting wear of a Hertzian line contact in partial slip. However, the simulation is not supported by an analytical solution, and the evolution of the wear volume with respect to the sliding distance is not thoroughly explained.

This work incorporates a fretting wear model for a 2D plane-strain contact using FEA (ANSYS 17.1) subject to force-controlled loading in the normal direction and displacement-controlled fretting motion in the tangential direction. Various COFs and the Archard wear model are applied at the interface. The FEA results are generalized by normalization, and fitted with empirical formulations. The initial gross slip distance is first defined. The Timoshenko beam theory and the tangential loading analysis of a half-elastic space are used to approximate the deflection of the half-cylinder and the block, respectively, supporting the empirical formulation. The wear volume under elastic conditions for a general cycle of the fretting motion is then derived based on the said function of the initial gross slip distance. In conclusion, the effect of plasticity on the wear volume is likewise investigated.

2. Model

The fretting model in this work is shown in Fig. 1. A simulated rigid plate is positioned on top of a half-cylinder that has a radius of R=0.5m, which is in contact with an R×4R block. The elastic modulus of that plate is set large enough (2×10^{10} GPa) to enforce a uniform downward displacement at the interface between the plate and half-cylinder during the fretting motion. That interface is made frictionless, as the rigid plate role is to prevent rotation of the half-cylinder at its upper boundary. The material of the half-cylinder and the flat block is first set to steel/steel, then to Alloy617/Alloy617, and finally to copper/copper. The material properties are listed in Table1. While the Poisson ratios of the chosen materials are very close, the moduli of elasticity and yield strengths are quite distinct.

The fretting loading condition is shown in Fig.1. The axes of X and Y are shown where the origin is located at the initial contact point. For brevity, the positive and the negative directions of X axis are metaphorically designated as “right” and “left”, respectively. The base of the flat block, a, is fixed in both the X and the Y directions (other B.C. will be discussed shortly). A normal force, P, is first applied to the top of the plate, which introduces a vertical interference, ω, designated as the indentation. With the normal force being kept constant, an oscillatory displacement in

the X direction, δ, is applied to the top of the half-cylinder. The oscillation magnitude in each cycle is maintained constant. That fretting cycles are identical to those in [17], but again for brevity, the schematics are omitted here. The loading condition is displacement-controlled in the X direction and force-controlled in the Y direction. In other words, the normal load, P, and the tangential displacement, δ, are inputs, while the interference, ω, and tangential force, Q, are outputs.

An Archard wear model, Eq. 1, is used at the contact between the half-cylinder and the block. The wear volume, V, is proportional to the normal force P, sliding distance, S, and inversely proportional to the hardness [12], H[1]. The hardness, H, is assumed to equal to $2.8*S_y$ for each material. The dimensionless wear coefficient K, according to Archard and Hirst [20], is typically between 10^{-2} and 10^{-5} for metallic contacts under unlubricated conditions. Without loss of generality, K is set to 10^{-4} in this work[2]. The Archard Wear Model is applied locally (i.e., at each nodal point) at the contact region.

$$V = \frac{KPS}{H} \tag{1}$$

1. Eq. (1) is used here as Archard intended, regarding hardness as a material property. According to the work by Jackson and Green [12], it has been shown that hardness actually depends not only on the yield strength but also on the deformation. For consistency with Archard original model, however, hardness is used here as if it were a constant material property.

2. A numerical value for K has to be implemented in the FEA code. However, because of normalization, the results are generalized for any value of K.

Journal of Applied Mechanics. Received January 08, 2019;
Accepted manuscript posted February 28, 2019. doi:10.1115/1.4043074

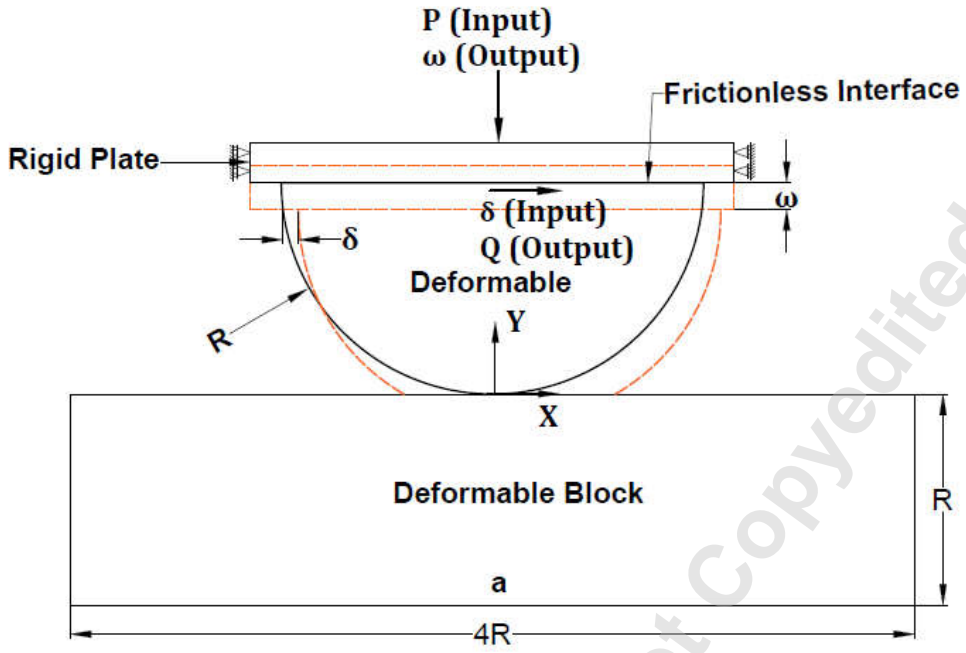

Figure 1: The loading condition and dimensions of the model

Table 1: The material properties and critical values for three cases [21].

Case	Materials	Elastic Modulus[GPa] E	Yielding Strength[MPa] S_y	Poisson Ratio ν	Critical Interference ω_c [μm]	Critical Load per Unit Length P_c/L [MN/m]	Critical Half Contact Width b_c [mm]
1	Steel	200	911	0.32	927	38.7	14.9
2	Alloy 617	211	322	0.3	144	4.83	5.26
3	Copper	130	331	0.33	328	7.90	8.30

2.1 Theoretical Equations for Normal Contact

For normal contact of elastic cylinders in plane-strain, the relations between the load per unit length, P/L, the half contact width, b, the maximum contact pressure, p_0, and the pressure distribution, p(x), are given in the following, according to the Hertzian theory of contact [9]:

$$p_0 = \frac{2P}{\pi bL} \tag{2}$$

$$b = \left(\frac{4PR}{\pi LE'}\right)^{\frac{1}{2}} \tag{3}$$

Journal of Applied Mechanics. Received January 08, 2019;
Accepted manuscript posted February 28, 2019. doi:10.1115/1.4043074

$$p(x) = p_0\sqrt{1-\frac{x^2}{b^2}} \tag{4}$$

The symbol ν represents the Poisson ratio, while E' represents the equivalent elastic modulus, given by:

$$\frac{1}{E'} = \frac{1-\nu_1^2}{E_1} + \frac{1-\nu_2^2}{E_2} = \frac{2(1-\nu^2)}{E} \tag{5}$$

The symbols, E_1 and E_2, correspond to the elastic moduli of the half-cylinder and the block, respectively, while ν_1 and ν_2 corresponds to the Poisson ratio of the half-cylinder and the block, respectively. In this work, $E=E_1=E_2$ and $\nu=\nu_1=\nu_2$, since the material properties of the two bodies in contact are set to be identical, with the outcome given in Eq. 5.

For the block whose depth equals to the radius of the half-cylinder, d=R=0.5m, the relation between the interference, ω, and the load per unit length, P/L, is derived by Yang and Green [17],

$$\omega = \frac{P/L}{2\pi E'}\left\{2\ln\left(\frac{2\pi RE'}{P/L}\right) - \frac{1}{1-\nu}\right\} \tag{6}$$

According to Green [14], the ratio between the maximum contact pressure and the maximum von-Mises stress is defined as a parameter, $C=p_0/\sigma_{emax}$. In the elastic contact regime, this parameter is a function of the Poisson's ratio, $C(\nu)=1.164+2.975\nu-2.906\nu^2$, for $\nu>0.1938$. By introducing this ratio, the critical half contact width, b_c, critical load per unit length, P_c/L, and critical interference, ω_c, at the onset of plasticity in the contact, are given by [14] and [17]:

$$b_c = \frac{2RCS_y}{E'} \tag{7}$$

$$\frac{P_c}{L} = \frac{\pi R(CS_y)^2}{E'} \tag{8}$$

$$\omega_c = \frac{R}{2}\left(\frac{CS_y}{E'}\right)^2\left[4\ln\left(\frac{\sqrt{2}E'}{CS_y}\right) - \frac{1}{1-\upsilon}\right] \tag{9}$$

By substituting the material properties in Table 1 into Eq.7-9, the critical values are then calculated and listed alongside. The three cases exhibit critical values that are quite distinct, which are nearly an order of magnitude different. The critical values in each cases are used to

Journal of Applied Mechanics. Received January 08, 2019;
Accepted manuscript posted February 28, 2019. doi:10.1115/1.4043074

normalize the foregoing results. It is also noted that the oscillation amplitudes in all cases are always maintained at $1*\omega_c$, which is listed in Table 1.

2.2 Theoretical Equations for Tangential Contact in the Elastic Regime

Consider the model in Fig.1 under a Hertzian pressure, p(x) (Eq. 4), caused by a total normal load per unit length, P/L (Eq. 2). A constant friction of coefficient (COF), μ, is applied to the contact when sliding takes place. According to Johnson [9], when the tangential traction per unit length, Q/L< μ*(P/L), the interface experiences partial slip conditions. As shown schematically in Figure 2, within the contacting region (-b<x<b), the conditions are stick for [-c, c], and slip between [-b, -c]U[c, b],. The symbol, c, is called the stick half-width.

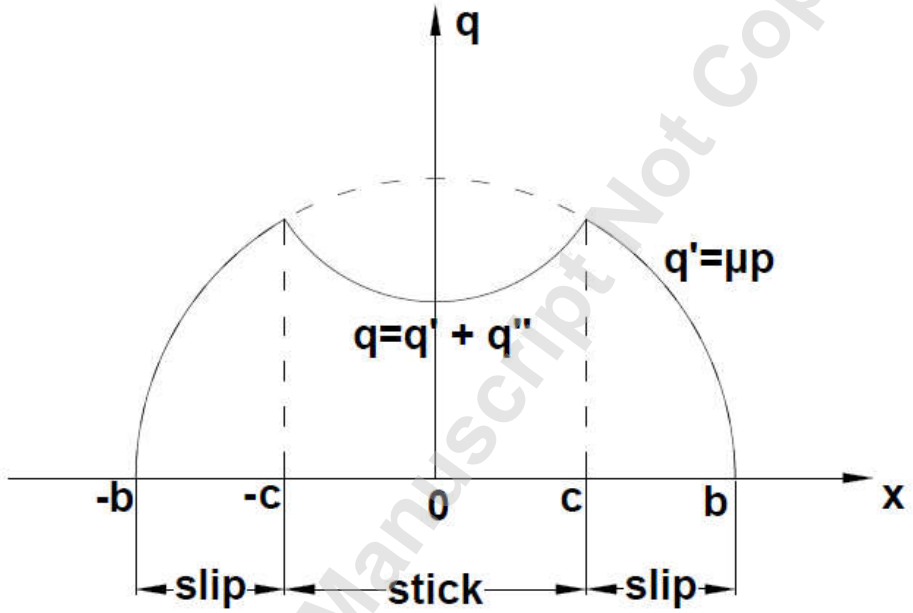

Figure 2: The distribution of tangential surface traction of the cylindrical contact under a tangential force, Q/L< μ(P/L).

In the slip region, the tangential traction is q'(x)=μp(x), where p(x) is the Hertzian pressure given by Eq.4. If the q'(x) is applied to the entire contact region, [-b, b], there should be another q''(x) to achieve the stick status for [-c, c], where all the points in the stick region displace uniformly. The distributions of q'(x) and q''(x) are given by Johnson [9],

$$q'(x) = \mu p_0 \sqrt{1-\frac{x^2}{b^2}} \qquad -b < x < b \tag{10}$$

$$q''(x) = -\frac{c}{b}\mu p_0 \sqrt{1-\frac{x^2}{c^2}} \qquad -c < x < c \tag{11}$$

Note that q(x)=q'(x) for slip region, and q(x)=q'(x)+q''(x) for stick region[3]. Clearly, the flat block and the half-cylinder always experience the tangential traction in opposite directions. For instance, if the half-cylinder is forced to the "right" (i.e., the positive X direction), in the coordinates of this model the flat block experiences q'(x) and q''(x), while the half-cylinder experiences –q'(x) and –q''(x).

When the tangential force per unit length reaches Q/L= μ(P/L), gross slip starts. In other words, the contact status is slip for the entire range [–b, b], while c=0. By taking the two bodies as two half elastic spaces, the tangential displacement on the surface of contact for each body, $\bar{u}(x)$, within contact is given by Johnson [9],

$$\bar{u}(x) = -\frac{(1-\nu^2)\mu p_0}{bE} x^2 \cdot \mathrm{sgn}(q(x)) + C \qquad -b < x < b \tag{12}$$

Hence, in the current coordinates, if the half-cylinder is forced to the "right", the tangential displacement of the half-cylinder, $\bar{u}_1(x)$, and that of the block , $\bar{u}_2(x)$, are, respectively:

$$\bar{u}_1(x) = \frac{(1-\nu_1^2)\mu p_0}{bE_1} x^2 + C_1 \qquad -b < x < b \tag{13}$$

$$\bar{u}_2(x) = -\frac{(1-\nu_2^2)\mu p_0}{bE_2} x^2 + C_2 \qquad -b < x < b \tag{14}$$

Considering the boundary condition that at the initial of gross slip, $\bar{u}_1(0) = \bar{u}_2(0)$, makes the two constants equal, $C_1=C_2$. The local sliding distance between the half-cylinder and the flat block at the initiation of the gross slip, $s_0(x)$, is then derived by $s_0(x) = \bar{u}_1(x) - \bar{u}_2(x)$. Using the relations, $E=E_1=E_2$ and $\nu= \nu_1= \nu_2$, gives,

$$s_0(x) = \frac{2(1-\nu^2)\mu p_0}{bE} x^2 \tag{15}$$

It is again emphasized that this initial gross slip equation is derived for elastic conditions.

3. Note that q(x) has units of stress and is occurring at the interface. It is distinguished from Q/L, which is the tangential force (per unit length) applied at the top of the half-cylinder, see Fig.1.

Journal of Applied Mechanics. Received January 08, 2019;
Accepted manuscript posted February 28, 2019. doi:10.1115/1.4043074

3. Mesh Convergence

Mesh convergence has been done to a displacement-controlled model by Yang and Green in [17]. However, since this model is force-controlled in normal direction and displacement-controlled in tangential direction, it is prudent to verify mesh convergence under such conditions just as well.

Element PLANE183 is used to mesh the model in ANSYS 17.1 (a representative of which is shown in Fig. 3). Taking the case for steel/steel for instance, there are 58103 elements for the entire model. The size of the refined mesh in the contact area is $8*10^{-4}R$. One hundred contact elements (CONTA172 and TARGE169) on each side of the contact are used to simulate the contact between the half-cylinder and the block. Similar mesh schemes are used to model the other two material cases.

A frictionless contact condition is applied to the interface between the rigid plate and the half-cylinder. The contact between the half-cylinder and the flat block is set to frictionless or frictional to investigate different cases. In the frictional contact cases, a small amount of fake slip is generated in sticking area to calculate tangential traction in ANSYS 17.1, and it is documented by ANSYS [22]. In order to alleviate the influence of this fake slip, the elastic slip tolerance factor is used so as to control the fake slip to be smaller than 1% of the sliding distance applied to the top of the half-cylinder.

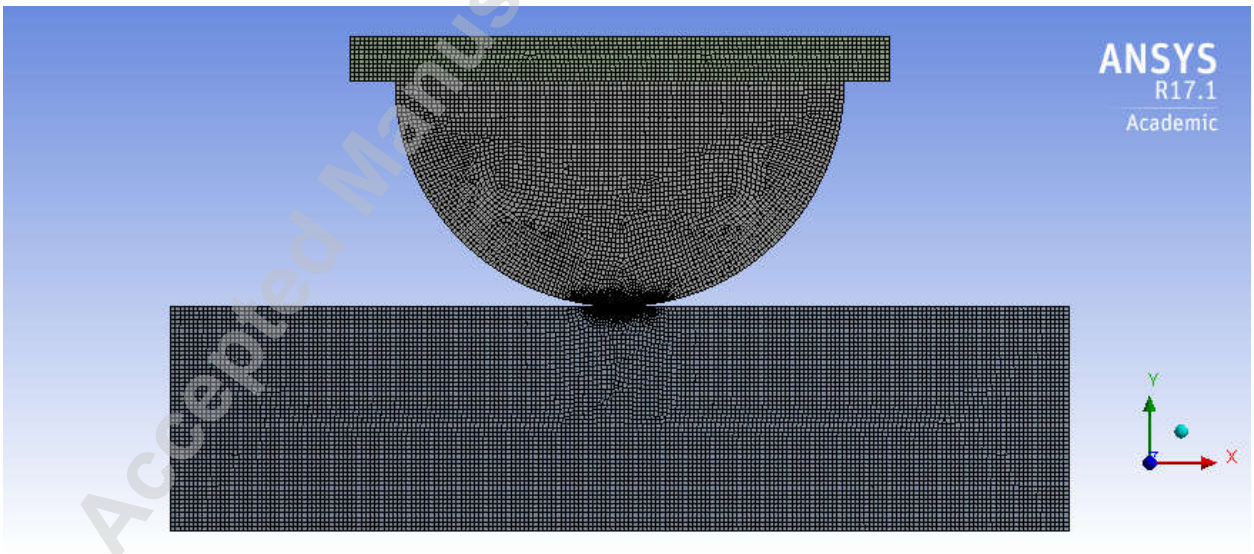

Figure 3: The model in ANSYS 17.1

Journal of Applied Mechanics. Received January 08, 2019;
Accepted manuscript posted February 28, 2019. doi:10.1115/1.4043074

The results of the mesh convergence for material Case1 (see Table 1) is shown in Table 2. It is first done to the pure normal elastic contact and frictionless loading. To validate the mesh in FEA, the results from ANSYS are compared with those obtained from theoretical predictions. With an input of normal force per unit length, P/L (ranges from 0.2*Pc/L to 1*Pc/L), the half contact width, b, is calculated by Eq. 3, and the interference, ω, is calculated by Eq. 6. The maximum contact pressure, p_0, is then derived by Eq. 2. The maximum von-Mises stress, $\sigma_{emax}=p_0/C$, is consequently obtained. The theoretical results for Case1 are compared with those from the finite element method (ANSYS 17.1), as shown in Table2. The percentage differences are listed under "%dif" for each of the parameters. Except for the difference of half contact width, b, that is 4.91% under 0.2 P_c due to the relative coarse mesh, all the other differences are below 3%. Table 3 shows the results for the case of P*=1, but for frictional loading with μ=0.3, for material Case 1. The half contact width converges to 15.2 mm after the mesh size is reduced to 0.8 mm and below (this is relative to the cylindrical radius of 500 mm). Note (from Table 2) that the theoretical value for the half contact width is 14.88 mm for frictionless contact. Clearly, further refinement of the mesh is unnecessary, and thus the mesh size of 0.4 mm is mostly adopted. Additionally, the region of contact is safeguarded to always be confined within the refined mesh. Similar mesh convergence processes for the other two material cases have also been done with similar outcomes. The mesh, therefore, can be regarded established for the elastic normal contact.

Table 2: Comparisons of contact parameters between theoretical predictions and FEA results for material Case1. The relation, $\sigma_{emax}=p_0/C$, is according to *Green [14]*.

Input	Theoretical Predictions					FEA Results							
		Eq. 6	Eq.3	Eq.2	p_0/C								
P^*	P/L [MN/m]	ω [μm]	b [mm]	p_0 [GPa]	σ_{emax}[GPa]	ω [μm]	%dif	b [mm]	%dif	p_0 [GPa]	%dif	σ_{emax}[GPa]	%dif
0.2	7.75	221	6.65	0.741	0.408	222	0.43	6.98	4.91	0.736	-0.72	0.410	0.56
0.6	23.2	590	11.52	1.28	0.706	591	0.13	11.75	2.00	1.28	-0.39	0.718	1.74
1	38.7	927	14.88	1.66	0.912	929	0.24	14.93	0.36	1.65	-0.16	0.930	2.03

Table 3: The half contact width for different mesh sizes in the contact region for a normal load, $P^*=1$, with elastic perfectly plastic model for material Case 1

Mesh Size in Contact region [mm]	8	4	2	0.8	0.4
Half Contact Width [mm]	16.0	15.7	14.5	15.2	15.2

Journal of Applied Mechanics. Received January 08, 2019;
Accepted manuscript posted February 28, 2019. doi:10.1115/1.4043074

Now, mesh convergence verification is done also for tangential loading. Under a tangential loading per unit length, $Q/L<\mu^*(P/L)$, the contact status is partial slip. At the inception of gross slip, the relative slip distribution (for the situation when the half-cylinder is forced to the right), $s_0(x)$, is given by Eq.15. That theoretical result is compared with those obtained from FEA.

Figure 4 shows the normalized local sliding distance under $P^*=1$ with $\mu=0.3$ at the inception of the gross slip for different pairs of materials. By inputting the normal load per unit length, P_c/L, the maximum contact pressure, p_0, and the half contact width, b, are obtained by Eqs. 2 and 3. With the known parameters, p_0, b, E, ν and μ, the sliding distance, $s_0(x)$, is derived by Eq.15 and normalized by the critical interference, ω_c. In the FEA model, $P^*=1$ is first applied to the top rigid plate, and then $1*\omega_c$ sliding distance to the "right" is stepwise applied to the top of the half-cylinder (see the stepwise details in [22]). By investigating the contact status during sliding, the gross slip starts at the sliding distance of $0.44*\omega_c$. The local sliding distance, $s_0(x)$, at $0.44*\omega_c$ is then obtained from ANSYS 17.1 as the local sliding distance at inception of the gross slip. The theoretical prediction agrees very well with the FEA results with a maximum difference less than 5% at the edges of the contact for all three cases. Note that Eq.15 shows symmetry with respect to x, and the FEA results confirm that behavior. The good agreement also exists for other material cases with different normal loads and different COFs, but for brevity, those results are omitted. With that verification, it is concluded that mesh convergence for elastic contacts is likewise established for tangential loading just as well.

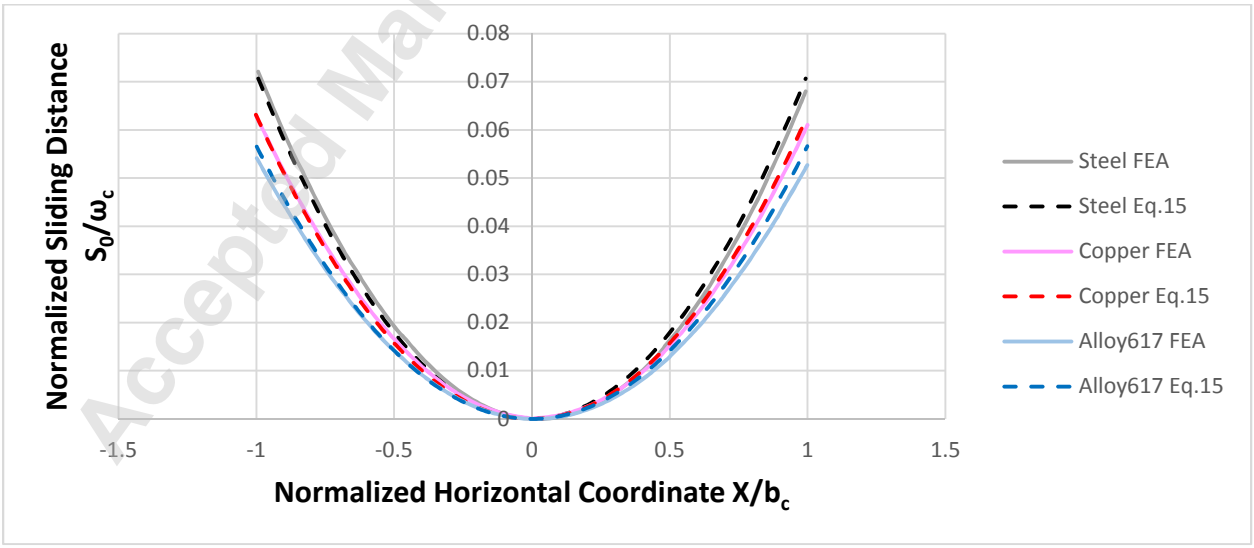

Figure 4: The normalized sliding distance at inception of gross slip under $P^*=1$ with $\mu=0.3$ for three material cases

Journal of Applied Mechanics. Received January 08, 2019;
Accepted manuscript posted February 28, 2019. doi:10.1115/1.4043074

Note that since there is no closed-form solution for elastic-plastic contacts under the combination of normal and tangential loads, the elements of the mesh are iteratively refined by a factor of two until there is less than one percent difference in the contact width between the iterations.

4. Results and Discussion

4.1 The initial gross slip distance

In the model of this work, after the normal load P/L is applied, the sliding distance, δ, is applied uniformly to every point on the top of the half-cylinder, as shown in Fig. 5. Before gross slip initiates, the sliding distance, δ, equals to the addition of the deflection of the half-cylinder, δ_1, and the tangential displacement of the stick region, δ_2, while the centerline of the half-cylinder, OA, deforms to O'A'. The deflection of the half-cylinder, δ_1, equals to the deflection of the centerline. The midpoint of the contact region is point, O, which is also the last point in stick just before gross slip starts. The tangential displacement of the stick region, δ_2, equals to the tangential displacement of the midpoint, O, to O', so $\delta_2=\overline{OO'}$.

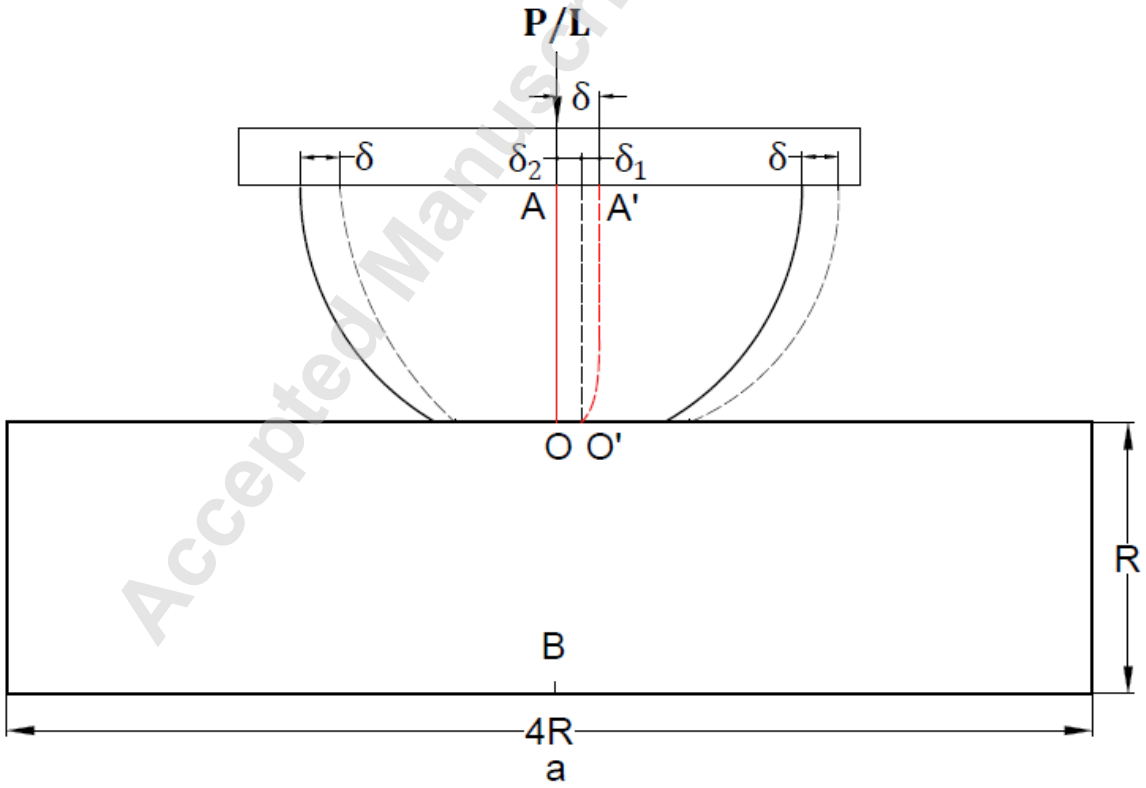

Journal of Applied Mechanics. Received January 08, 2019;
Accepted manuscript posted February 28, 2019. doi:10.1115/1.4043074

Figure 5: The schematic of the sliding distance

For the frictional contact under partial slip condition, as the sliding distance, δ, increases, the tangential traction, Q/L increases with it. When Q/L=μ(P/L), the onset of gross slip begins. The corresponding sliding distance is designated to the initial gross slip distance, δ_i. That δ_i varies under different P/L and different COFs. Figure 6 shows both the FEA results and theoretical predictions for the evolutions of the normalized initial gross slip distance, δ_i/ω_c, with different P^* and μ for steel/steel. The inset of the figure shows the same results but in linear scale coordinates. The δ_i is shown to be proportional to P/L and μ. A fitting function is found to express δ_i analytically as:

$$\delta_i = 4.78\mu^{1.15}\left(\frac{P/L}{RE}\right)^{0.928} R \tag{16}$$

The rationale for this fit-form is forthcoming (details are provided below and in the Appendix).

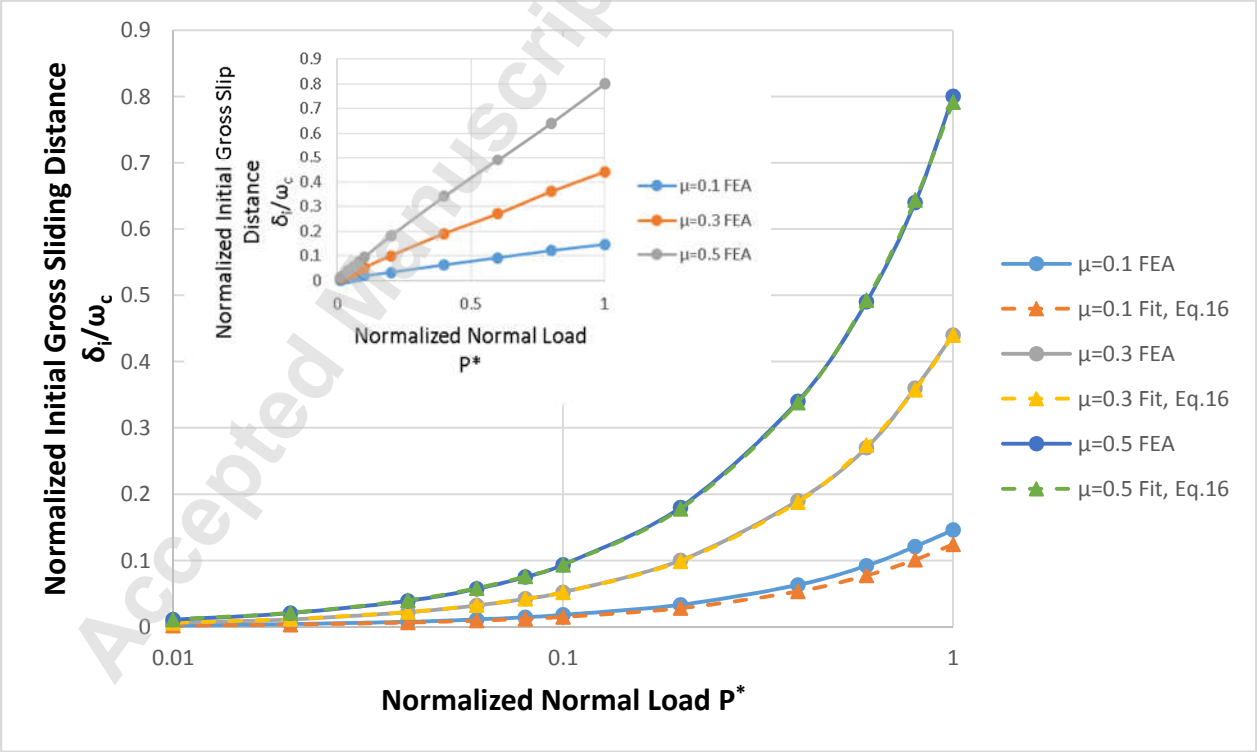

Figure 6: The normalized initial gross slip distance under different normalized normal loads with different COFs for the FEA results and fitting functions, Eq.16, for steel/steel

Journal of Applied Mechanics. Received January 08, 2019;
Accepted manuscript posted February 28, 2019. doi:10.1115/1.4043074

The predicted normalized initial gross slip distance from the fitting function in Eq.16 is compared with the results from FEA, as shown in a semi-log scale of Fig.6. The normalized load is given in log scale in order to spread the data points at low P^*. The results from the FEA and the fitted function agree well with the maximum difference of less than 5%. Noteworthy, Figure 7 shows the dimensional initial gross slip distance under μ=0.3 and different normal loads for three different pairs of material for R=0.5m, and for steel/steel also for three radii R=0.05m, 0.5m, and 5m. The normal load for each material ranges from $0.01*P_c/L$ to $1*P_c/L$. While the three materials are vastly different in material properties as listed in Table1, the results from the FEA and the fitted function agree well with less than 5% difference even when the radii are orders of magnitude different. Therefore, in the foregoing Eq. 16 is used to predict the initial gross slip distance.

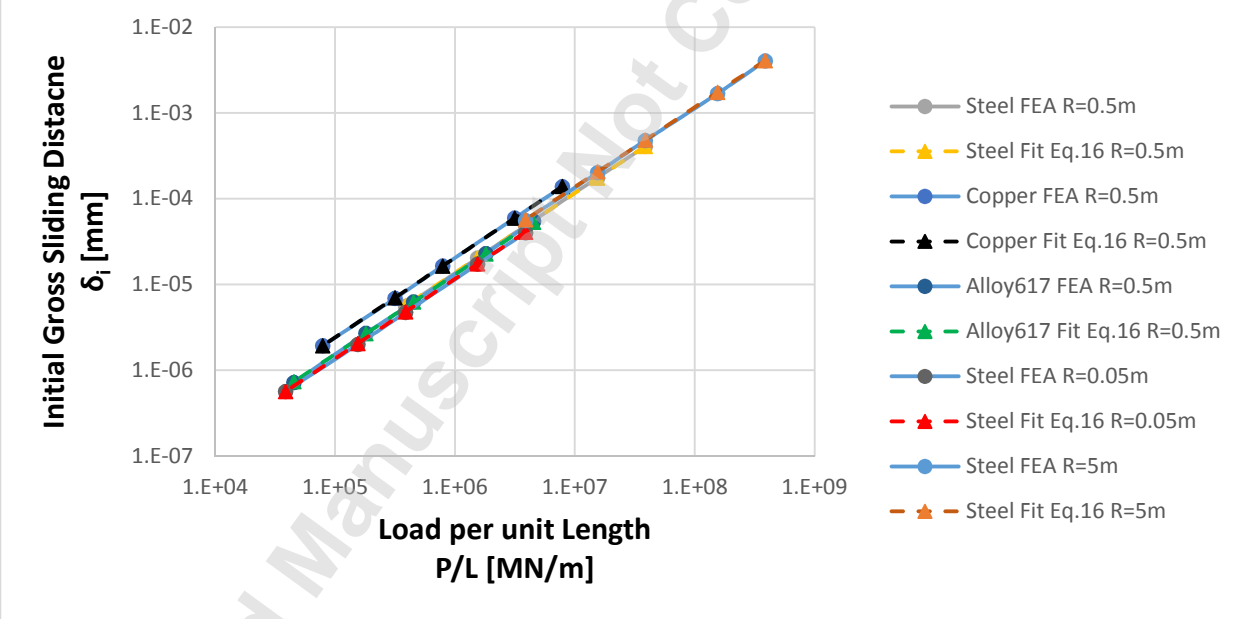

Figure 7: The dimensional initial gross slip distance under different normal loads with μ=0.3 for the FEA results and fitting functions results for steel/steel (for R=0.05m, 0.5m and 5m), for Alloy617/Alloy617, and for Cu/Cu (for R=0.5m)

The initial gross slip, δ_i, as given by Eq.16, seems nearly linearly proportional to μ and P/L. That is explained in the Appendix with the Timoshenko beam theory and half-elastic space loading analysis. The deflection of the half-cylinder, δ_{i1}, where the gross slip initiates is obtained in the Appendix, specifically see Eq. A8. By nullifying the unknown but small moment on the tips, $M_0/L=0$, the deflection of the half-cylinder can be estimated.

Journal of Applied Mechanics. Received January 08, 2019;
Accepted manuscript posted February 28, 2019. doi:10.1115/1.4043074

Figure 8 shows the deflections of the half-cylinder at the initiation of gross slip from FEA and Eq. A8 (with M_0/L being neglected as discussed in the Appendix), for $P^*=1$ at three different COFs. While the results from both seem to converge for small COFs, the difference increases with the COFs, which cause larger tangential loads and strains. Recall that the strain-displacement relation in the Timoshenko beam analysis is valid for small strains. Consequently, that is the cause for the discrepancy.

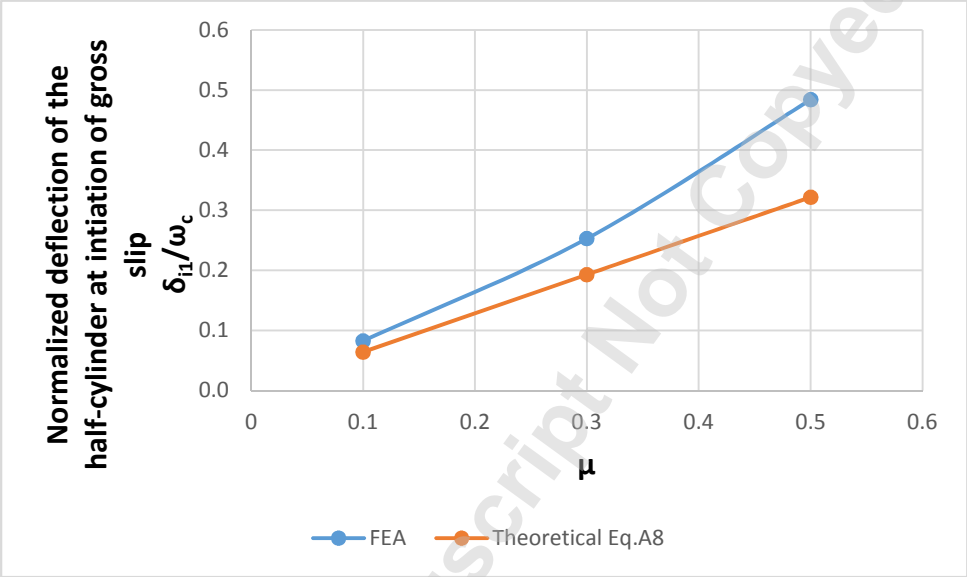

Figure 8: The deflections of the half-cylinder at the initiation of gross slip from FEA and Eq. A8 with for $P^*=1$ at different COFs

The tangential displacement, δ_{i2}, can be estimated by taking the block as a half elastic space and applying the Hertzian distributed tangential traction to the contacting region. The tangential displacement distribution, u(x), on the surface is derived by Eq. A18. Figure 9 shows the u(x) from FEA and Eq. A18 at $P^*=1$ with μ=0.3. The results agree well on the "left" side of the surface with little difference at the contact center. A larger difference appears on the "right" side, since the boundary condition of the right side of the block is free, so the block does not produce sufficient resistance to horizontal deflection. The difference is likewise heightened by ignoring the normal load, p(x), when calculating u(x). Fortunately, though, the tangential displacement, δ_{i2}, is relevant only on the "left" part (x<0) of the surface anyhow. Therefore, the estimation in Eq. A19 is unaffected by the differences shown in the behavior on the "right" side. Noteworthy, Eq. A8 and A19 that estimate δ_{i1} and δ_{i2}, respectively, are nearly linearly proportional to μ and P/L, which provides the rationale for Eq. 16. The slight deviation

Journal of Applied Mechanics. Received January 08, 2019;
Accepted manuscript posted February 28, 2019. doi:10.1115/1.4043074

from linearity is caused by the difference in the boundary conditions used in the FEA pitted against the half-space assumption used in the analytical model.

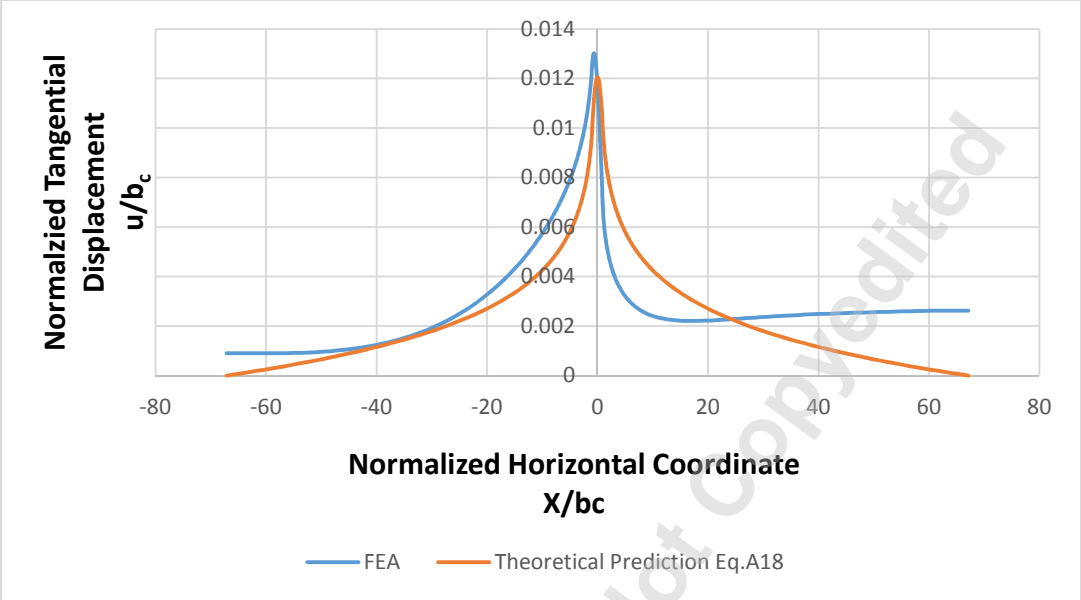

Figure 9: The tangential displacement on the surface of the block at $P^{\cdot}$=1 with μ=0.3 from FEA and half elastic space estimation

4.2 The wear volume at initiation of gross sliding

As discussed in section 2.2, before gross sliding starts, the contact condition is partial slip and partial stick, as shown in Fig.2. The local Archard Wear model is applied to the interface, as given by:

$$v(x) = \frac{K}{H} p(x) s(x) \tag{17}$$

Here, only the wear on the half-cylinder is considered. The local wear volume, v(x), is proportional to the dimensionless wear coefficient, K, contact pressure, p(x), and the local sliding distance, s(x), while it is inversely proportional to the hardness, H. Clearly, wear happens in both the half-cylinder and the block, in which case the wear volume is just twice that of the case for half-cylinder alone. This is true for identical materials in contact. Had the materials been different, the wear volume would be inversely proportional to the hardness. Note that the evolution of the contacting profile due to wear is not considered here.

At the initiation of gross sliding, the local sliding distance is $s(x)=s_0(x)$, as given by Eq. 15. The pressure distribution can be approximated by the Hertzian pressure, p(x), as given by Eq. 4. The total wear volume at the initiation of gross sliding, V_0, can be derived by integrating Eq. 17 over the region in contact:

Journal of Applied Mechanics. Received January 08, 2019;
Accepted manuscript posted February 28, 2019. doi:10.1115/1.4043074

$$V_0 = \int_{-b}^{b} \frac{K}{H} p(x) s_0(x) dx = \int_{-b}^{b} \frac{K}{H} p_0 \sqrt{1-\frac{x^2}{b^2}} \frac{2(1-\nu^2)\mu p_0}{bE} dx \tag{18}$$

The result of the Eq. 18 gives the wear volume at the initiation of gross slip, giving:

$$V_0 = \frac{(1-\nu^2)\mu\pi K p_0^2 b^2}{4HE} \tag{19}$$

In order to normalize the results, the critical wear volume, V_c, is defined as:

$$V_c = \frac{K_c \omega_c (P_c / L)}{H} \tag{20}$$

Herein, the critical wear coefficient is by definition, K_c=1.

Figure 10 shows the normalized wear volume at the initiation of gross slip, V_0/V_c, from FEA and Eq. 19 at different normal loads and COFs for steel/steel. Since the tangential displacement is applied stepwise, it is hard to pinpoint numerically the initiation of gross slip. Conversely, the two steps changing from partial slip to gross slip are easy to detect. Thus, V_0 in the FEA is decided as the average volume between these two steps. As shown in Fig. 10, the results in the FEA and from Eq. 19 agree very well with less than 5% difference, which further verifies the theoretical prediction.

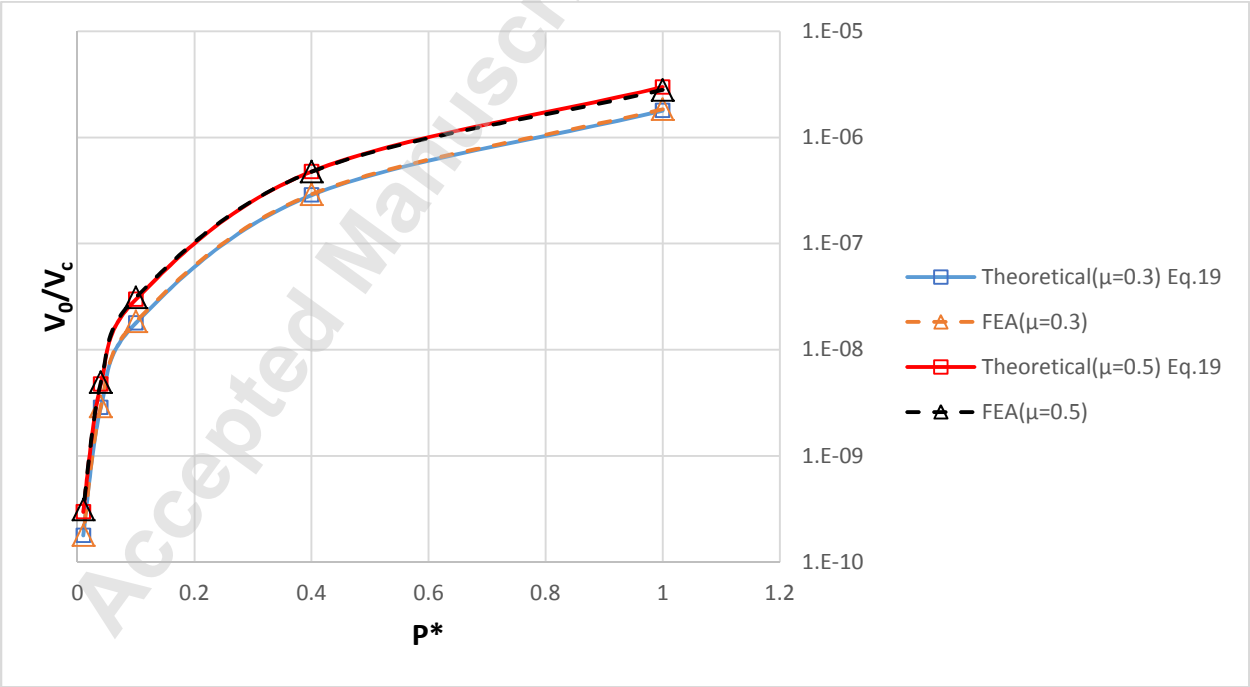

Figure 10: the normalized wear volume at the initiation of gross slip, V_0/V_c, from FEA and Eq. 19 at different normal loads and COFs with $K=10^{-4}$ for steel/steel

Journal of Applied Mechanics. Received January 08, 2019;
Accepted manuscript posted February 28, 2019. doi:10.1115/1.4043074

Figure 11 shows the wear volume at the initiation of gross slip, V_0, from FEA and Eq. 19 with μ=0.3 now for different material pairs. The normal load for each material ranges from $0.01*P_c/L$ to $1*P_c/L$. The results for the three cases from the FEA and Eq. 19 are all in excellent agreement with less than 5% difference, which supports the viability of using Eq. 19 for different material pairs.

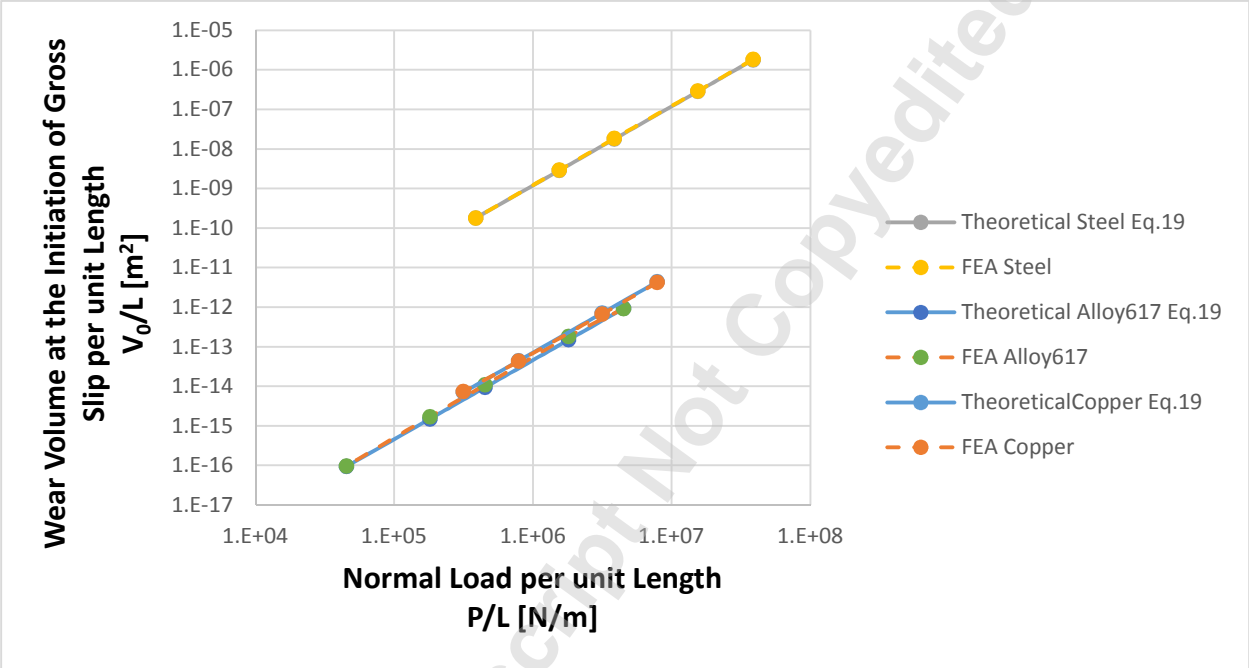

Figure 11: the normalized wear volume at the initiation of gross slip, V_0/V_c, from FEA and Eq.19 at different normal loads with μ=0.3 for Steel/Steel, Alloy617/Alloy617, and Copper/Copper

4.3 Prediction of fretting wear volume under elastic conditions

During the fretting motion, the amplitude of each cycle in the different cases (see Table 1) is maintained at $1*\omega_c$. Figure 12 shows the typical evolution of wear volume during one cycle of the motion from FEA results at P^*=1 with different COFs for steel/steel under elastic conditions. The nominal sliding distance, S_n, represents the cumulative tangential sliding distance applied to the top surface of the half-cylinder, which is different from the local sliding distance at the contact region. It is also different from δ, which is the tangential displacement applied to the top surface of the half-cylinder. For μ=0, the wear volume increases linearly with respect to the nominal sliding distance, and it is a special case for gross slip fretting. For μ=0.3, there are two parts in each direction of sliding (the half-cylinder changes direction at $S_n^*=S_n/\omega_c$=1, 3, etc.). At the beginning, the contact status is

Journal of Applied Mechanics. Received January 08, 2019;
Accepted manuscript posted February 28, 2019. doi:10.1115/1.4043074

partial slip and the wear volume increases slowly. As the half-cylinder displaces further, gross slip starts and the wear volume increases linearly at the same rate as that in the case of μ=0. For μ=1, the contact status is always partial slip with no gross slip. Thus the wear volume is thus negligible compared with the other two cases. In this work, the prediction of the wear volume is only done for the case when gross slip condition is reached.

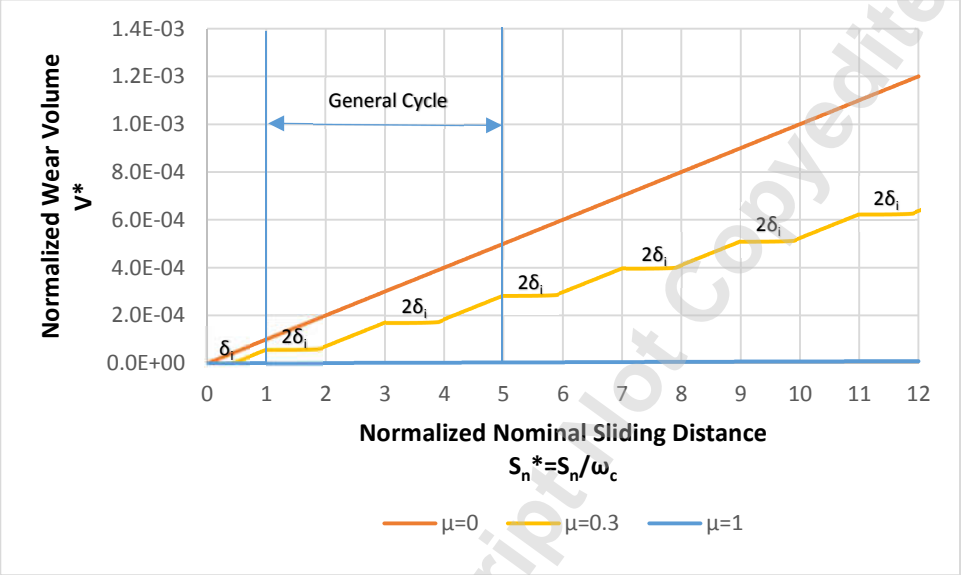

Figure 12: The FEA results of the evolution of normalized wear volume during three cycles of fretting motion at P^*=1 for steel/steel in elastic contact

For the case with μ=0.3 as shown in Fig.12, the evolution of the wear volume is periodic after S_n^*=1. Hence, a general cycle is presented in the figure, starting where the half-cylinder is positioned at the rightmost point, i.e., x^*=1 or S_n^*=1, heading back to the leftmost position, i.e., x^*=-1 or S_n^*=5, thus completing a general cycle. Then, the half-cylinder changes motion returning to the rightmost position.

The wear volume for a general cycle is thus analyzed by taking the cycle, S_n^*=1 to 5, for instance. At the beginning of the cycle (S_n^*=1), the half-cylinder is at the rightmost position, x^*=1. Since the half-cylinder is forced to the right before reaching S_n^*=1, its centerline is pre-deflected by a tangential force acting to the right. At the beginning of the cycle, the half-cylinder starts to move to the left. The centerline of the half-cylinder now restores and deforms from the right to the left. As a result, it takes a nominal sliding distance $2\delta_i$ (i.e., $S_n=2\delta_i$) to finish the partial slip condition, with a corresponding wear volume that is $V=2V_0$. As the half-cylinder slides further to the left, gross slip starts, i.e., the nominal sliding

Journal of Applied Mechanics. Received January 08, 2019;
Accepted manuscript posted February 28, 2019. doi:10.1115/1.4043074

distance equals to the sliding distance in the contact region, $s(x)=\Delta S_n$. The normalized wear rate, i.e., the slop of the normalized wear volume in Fig. 12, for gross slip is:

$$\frac{\Delta V^*}{\Delta S_n^*}=\frac{\int_{-b}^{b}\frac{Kp_0(x)\Delta S_n dx}{H}\Big/\frac{KP_c\omega_c}{H}}{\Delta S_n/\omega_c}=K\frac{\int_{-b}^{b}p_0(x)dx}{P_c}=KP* \tag{21}$$

Here, $\Delta V^*=\Delta V/V_c$, $\Delta S_n^*=\Delta S_n^*/\omega_c$.

When the half-cylinder returns back to the right at $x^*=0$ or $S_n^*=3$, the second partial slip starts with $V=2V_0$. After that, another gross slip begins with the normalized wear rate given by Eq.21. The total wear volume for a general cycle during partial slip condition is thus:

$$V_{partial}^*=4V_0^* \qquad \delta_i^*<0.5 \tag{22}$$

The total normalized nominal sliding distance for the gross slip condition during a general cycle is, $\Delta S_n^*=4(1-\delta_i^*)$. Then, the total wear volume for the gross slip condition during a general cycle is:

$$V_{slip}^*=\Delta S^*\frac{\Delta V^*}{\Delta S^*}=4(1-\delta_i^*)KP^* \qquad \delta_i^*<0.5 \tag{23}$$

The normalized wear volume for a general cycle of the fretting motion is then the sum of $V^*_{partial}$ and V^*_{slip}:

$$V^*=4V_0^*+4(1-\delta_i^*)KP^* \qquad \delta_i^*<0.5 \tag{24}$$

If $\delta_i^*>0.5$, the partial slip condition will last for the whole cycle, which leads to a very small (negligible) wear volume.

Figure 13 shows the normalized wear volume for a general cycle of fretting motion under elastic condition with different normal loads and COFs for steel/steel. The results from FEA and Eq.24 agree very well, which further verifies the theoretical predictions. For the case with μ=0.5, the wear volume first increases with the normal load as predicted by the Archard Wear model. However, the wear volume decreases as the normal load further increases, because δ_i^* increases with P^*, which then decreases V^*, as shown in Eq.24.

Figure 14 shows the results of the wear volume for a general cycle of fretting motion under elastic condition with μ=0.3 under different normal loads, now for three different material

Journal of Applied Mechanics. Received January 08, 2019;
Accepted manuscript posted February 28, 2019. doi:10.1115/1.4043074

cases (see Table 1). The results from the FEA and theory are in very good agreement, which further verifies the analytical predictions.

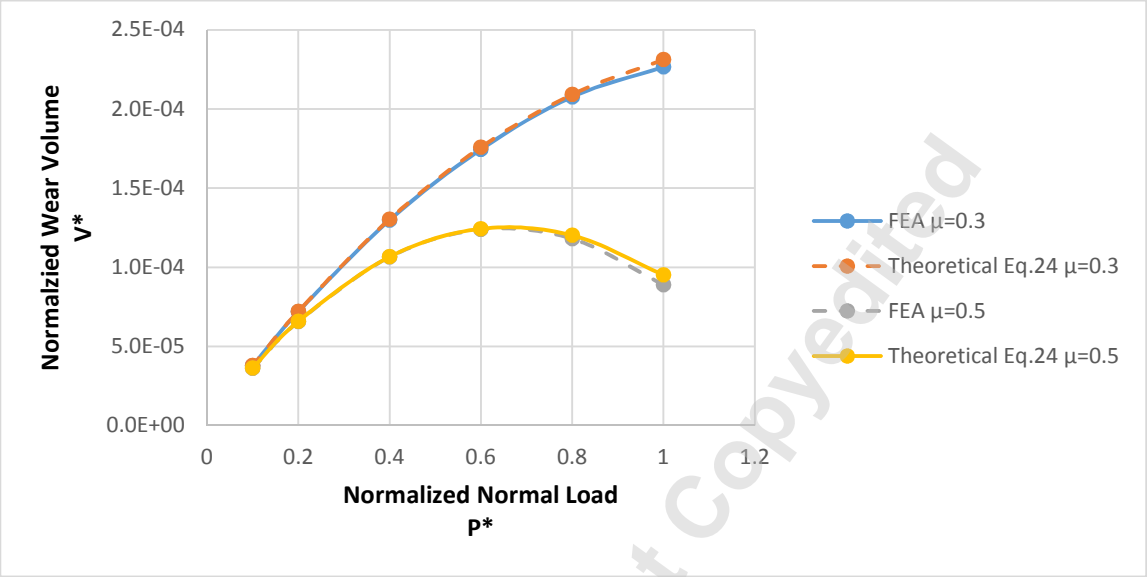

Figure 13: The wear volume for a general cycle of fretting motion at elastic condition for different normal loads and COFs, comparing FEA and theoretical predictions for steel/steel (for R=0.5m)

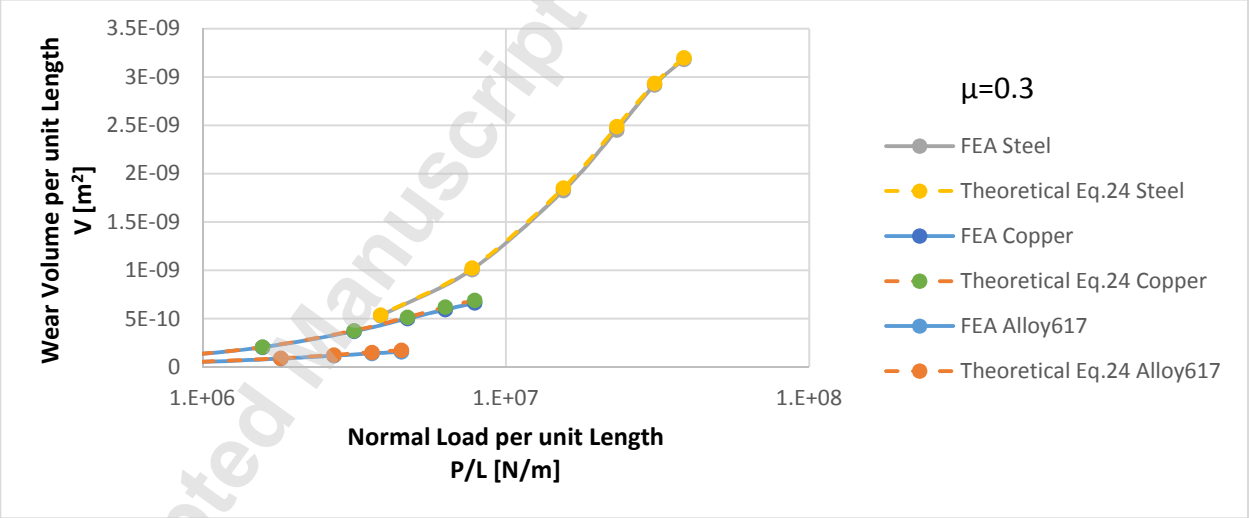

Figure 14: The wear volume for a general cycle of fretting motion at elastic condition with μ=0.3 under different normal loads from FEA and theoretical predictions for steel/steel, Alloy617/Alloy617, and Copper/Copper (for R=0.5m)

4.4 The effect of plasticity

In the previous section, the wear volume is considered for elastic conditions. Here, the elastic perfectly-plastic contact model is applied. To find the influence of plasticity on the wear volume, two groups of loading conditions are compared. One is the loading that introduces plasticity, and the other is the same loading but yielding (or plasticity) is disabled

Journal of Applied Mechanics. Received January 08, 2019;
Accepted manuscript posted February 28, 2019. doi:10.1115/1.4043074

(i.e., pure elasticity is open-endedly imposed upon the material in ANSYS 17.1, as it is solved in Section 4.3). The wear volumes between the elastic and plastic conditions are then compared in Fig. 15. Figure 15 shows the evolution of wear volume at P^*=1 with different COFs under elastic and elasto-plastic conditions. Plasticity appears due to the combined effects of normal and the frictional tangential loadings. The wear volumes under pure elastic conditions are larger than those under elasto-plastic conditions in these two cases. For μ=0.3, there is larger tangential deflection in the elasto-plastic case, which decreases the gross slip distance and the wear rate during gross slip. Consequently, the wear volume in the elasto-plastic case is smaller. For μ=0.5, the decrease of wear volume in the elasto-plastic condition is dominated by the junction growth effect (see details in [17]). Due to the large COF, higher plastic strains (deformations) are generated at the interface, causing an increase of the contact region, i.e., causing junction growth. The junction growth leads to the partial slip condition at the two limit positions during the fretting motion, which greatly decreases the wear volume.

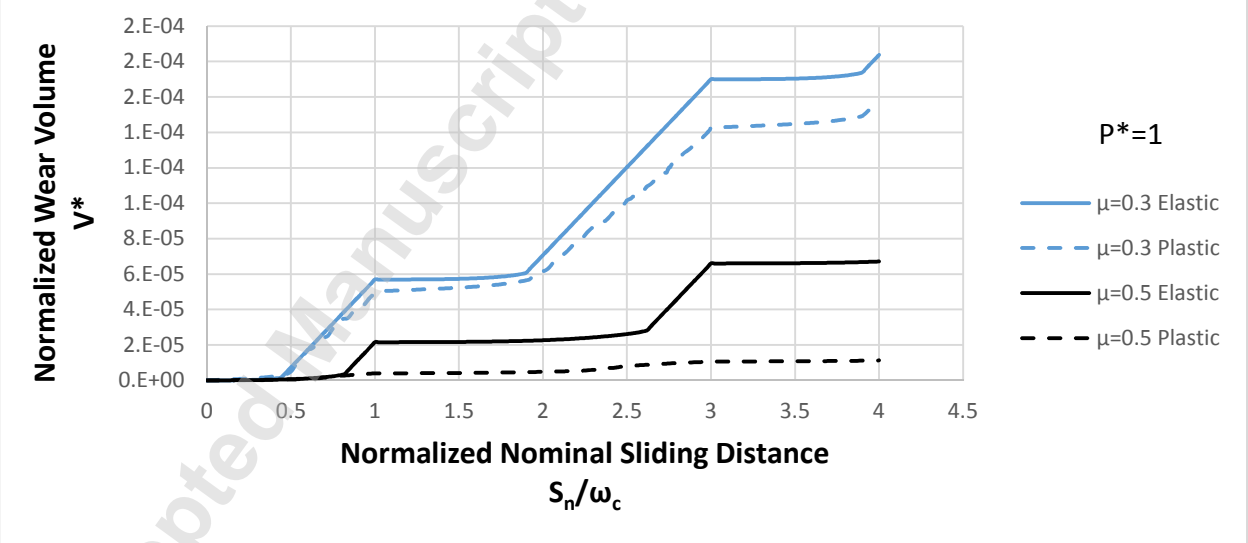

Figure 15: The evolution of wear volume at elastic and plastic conditions with different COFs under P^*=1 for steel/steel during one cycle of fretting motion (for R=0.5m).

It should be noted that the wear volumes in elastic cases are not always larger than those in elasto-plastic cases under the same loading conditions. As shown in Fig.16, the wear volume at P^*=3 with μ=0.3 is larger in elastic case first, but larger in elasto-plastic case after three-fourth of the cycle that keeps getting larger up to three cycles, which is the largest number of the cycle in the current simulation. Wear is larger in the elastic case first, because

Journal of Applied Mechanics. Received January 08, 2019;
Accepted manuscript posted February 28, 2019. doi:10.1115/1.4043074

plasticity introduces junction growth, which decreases the sliding distance at the interface with the same amount of nominal sliding distance. It is larger in the elasto-plastic case afterwards because the cross section, A(x), given in Eq. A3, is getting larger in elasto-plastic contact, which decreases the deflection. Consequently, the sliding distance at the interface is larger with the same amount of nominal sliding distance.

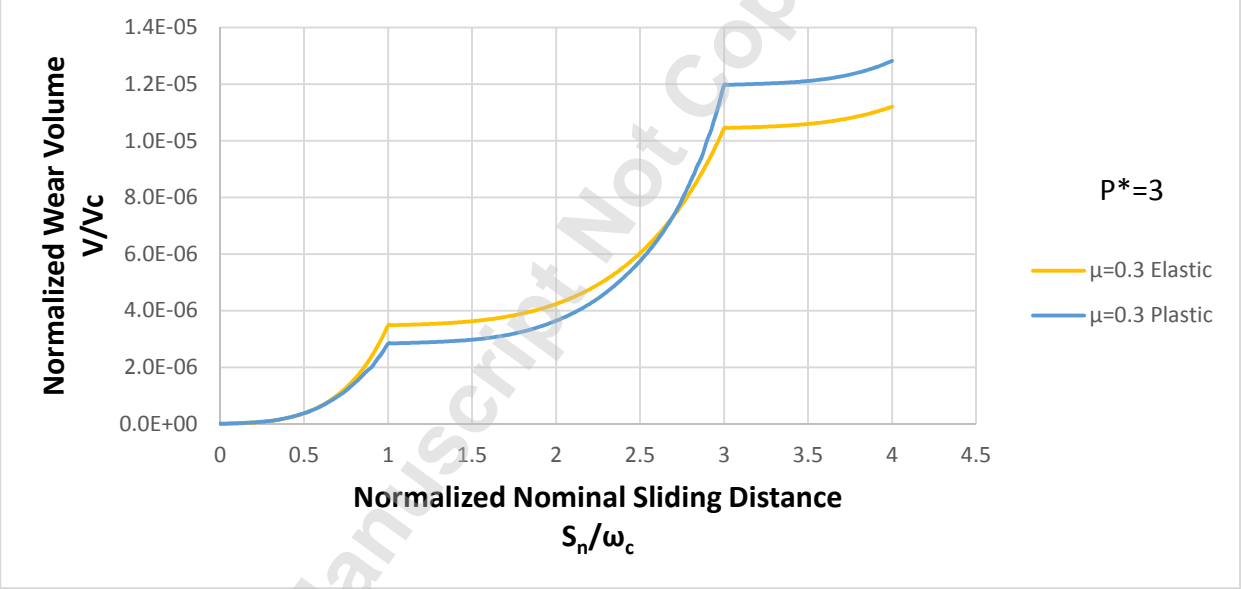

Figure 16: The evolution of wear volume at elastic and plastic conditions with μ=0.3 under P^*=3 for steel/steel during one cycle of fretting motion.

5. Conclusion:

A fretting wear model is presented in this work for a cylindrical line contact, under 2D plane-strain conditions, for force-controlled in the normal direction and displacement-controlled in the tangential direction. Friction and the Archard wear model are applied at the interface. Three different material pairs are examined by the model. The following are the outcomes:

1.The initial gross slip distance is defined and approximated with the Timoshenko beam theory and line loading of a half elastic space. A fitting function for the initial gross sliding

distance is also derived. Both the theoretical approximation and the fitting function agree well with the FEA results.

2. The wear volume at the initiation of the gross slip is derived. Results between the theoretical prediction and FEA are in good agreement.

3. The wear volume under elastic conditions for the first cycle of the fretting motion is derived based on the fitting function of the initial gross sliding distance. The results are in good agreement between the theoretical predictions and the FEA.

4. The effect of the plasticity is analyzed. On one hand, under small normal load plasticity introduces small deflections and junction growth when COFs are large. These two effects decrease the wear volume. On the other hand, under larger normal loads plasticity introduces larger cross sections, which makes the two bodies stiffer to the tangential load. As a result, the deflection decreases, and the wear volume increases.

6. Acknowledgement

This research is supported by the Department of Energy under Project 2506U87, Award RH452. This support is gratefully acknowledged.

Appendix

The initial gross sliding distance for elastic contacts can be estimated by regarding the half-cylinder as a Timoshenko beam[4] while assuming the block as a half elastic space. The loading condition of the half-cylinder is shown in Fig.17, when gross slip initiates, i.e., when $Q/L=\mu(P/L)$. In addition to Q/L, there is also a moment per unit length, M_0/L, acting about the tip of the half-cylinder. This moment, M_0/L, is caused by the curvature of the contacting surface, and the local tangential traction $\mu p(x)$ (as shown in Fig. 17b). This moment is directly related to μ and P/L. The moment distribution, M(x)/L, the second moment of area, I(x)/L, and the cross section area, A(x)/L, are given, respectively, by:

[4] The Timoshenko beam is appropriate for thick or short beams, since it accounts for shear deformation and rotational bending effects.

Journal of Applied Mechanics. Received January 08, 2019;
Accepted manuscript posted February 28, 2019. doi:10.1115/1.4043074

$$\frac{M(x)}{L}=\mu\frac{P}{L}(R-x)+\frac{M_0}{L} \tag{A1}$$

$$\frac{I(x)}{L}=\frac{2}{3}(R^2-x^2)^{\frac{3}{2}} \tag{A2}$$

$$\frac{A(x)}{L}=2(R^2-x^2)^{\frac{1}{2}} \tag{A3}$$

According to the Timoshenko beam theory [23], the angle of rotation of the mid-surface is defined as φ. The derivative of φ is determined by M(x)/L and I(x)/L according to:

$$\frac{M(x)}{L}=-E\frac{I(x)}{L}\frac{d\varphi}{dx} \tag{A4}$$

By integrating Eq. A4 with the boundary condition, φ=0 at x=0, the distribution of φ is expressed as:

$$\varphi(x)=\frac{3}{2}\frac{\mu P}{REL}\left[\frac{R-(1+\frac{M_0}{\mu RP})x}{\sqrt{R^2-x^2}}-1\right] \tag{A5}$$

According to the Timoshenko beam theory [23], the derivative of the deflection of half-cylinder, Δ, is related to φ by:

$$\frac{d\Delta}{dx}=\varphi-\frac{1}{kAG}\frac{d}{dx}(EI\frac{d\varphi}{dx}) \tag{A6}$$

By substituting φ(x) from Eq. A5 into Eq. A6, the distribution of deflection of the half-cylinder, Δ, can be solved by integrating Eq. A6 with the boundary condition, Δ=0 at x=0. The expression of Δ(x) is thus:

$$\Delta(x)=\frac{3}{2}\frac{\mu P}{EL}[\arcsin(\frac{x}{R})+(1+\frac{M_0}{\mu RP})\frac{\sqrt{R^2-x^2}-R}{R}-\frac{x}{R}] -\frac{\mu P}{2kGL}\arcsin(\frac{x}{R}) \tag{A7}$$

The deflection of the half-cylinder at the initiation of gross slip, δ_{i1}, can be estimated by taking the deflection of the tip of the beam, $\delta_{i1}=\Delta(R)$. That is given by:

Journal of Applied Mechanics. Received January 08, 2019;
Accepted manuscript posted February 28, 2019. doi:10.1115/1.4043074

$$\delta_{i1} = |\Delta(R)| = [\frac{3\mu P}{4EL}(4-\pi) + \frac{3M_0}{2EL} + \frac{\pi\mu P}{4kGL}] \quad \text{(A8)}$$

Here, the Timoshenko shear coefficient, k, for rectangular cross section is taken according to Cowper [24], as:

$$k = \frac{10(1+\nu)}{12+11\nu} \quad \text{(A9)}$$

and the shear modulus, G, is given by:

$$G = \frac{E}{2(1+\nu)} \quad \text{(A10)}$$

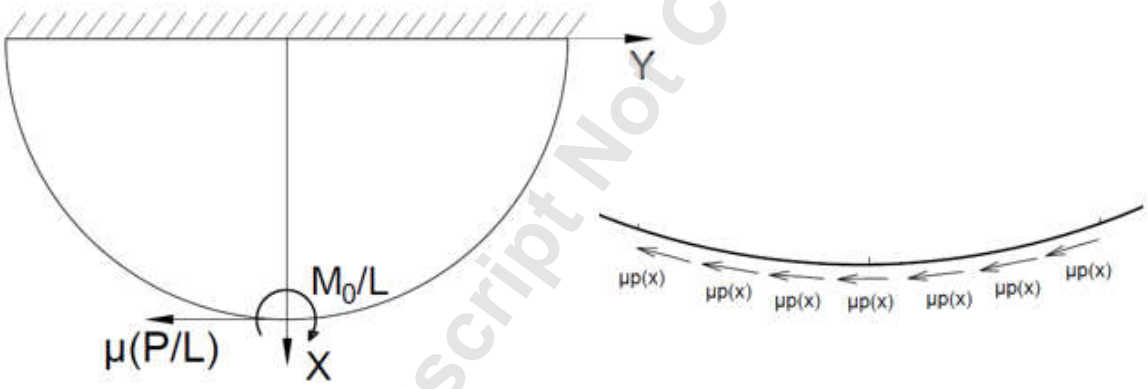

(a) (b)

Figure 17: (a) The loading condition of the half-cylinder as a Timoshenko beam at slip onset (b) Zoomed in contact region

The influence of the moment, M_0/L, on δ_{i1} is analyzed in now the following. The moment is maximum when the half-cylinder is undeformed (the curvature of the tip is maximum, as if the normal load does not deform the tip of the half-cylinder). Hence, the maximum moment, M_0/L, can be estimated using Fig. 18. The contact region, $-b<x<b$, is confined to a corresponding angle range, $-\theta_0<\theta<\theta_0$, where θ_0 is given by:

$$\theta_0 = \arcsin\frac{b}{R} \quad \text{(A11)}$$

Journal of Applied Mechanics. Received January 08, 2019;
Accepted manuscript posted February 28, 2019. doi:10.1115/1.4043074

The local frictional force in this region is q(x)=μp(x). The arm of the force is represented by the length of $\overline{OC}$ in Fig.18, and is given by:

$$\overline{OC} = 2R\sin^2\frac{\theta}{2} \tag{A12}$$

The moment on the tip of the half-cylinder, M_0/L, can be estimated by integrating the product of the local friction force and the arm of the force:

$$M_0 / L = \int_{-b}^{b} \mu p(x) 2R\sin^2\frac{\theta}{2} dx = \int_{-\theta_0}^{\theta_0} 2\mu p_0 \sqrt{1-(\frac{R\sin\theta}{b})^2} R^2 \sin^2\frac{\theta}{2} d\theta \tag{A13}$$

In the case where θ is small, which agrees with the conditions here (θ~0.01 rad), Eq. A13 can be simplified as:

$$M_0 / L = \frac{\mu\pi p_0 b^3}{16R} \tag{A14}$$

According to the above estimation, the deflection of half-cylinder caused by the M_0/L is found to be less than 0.1% of the total deflection for different material cases and different normal loads with different COFs. Therefore, the moment on the tip of the half-cylinder, M_0/L, can largely be ignored in the foregoing.

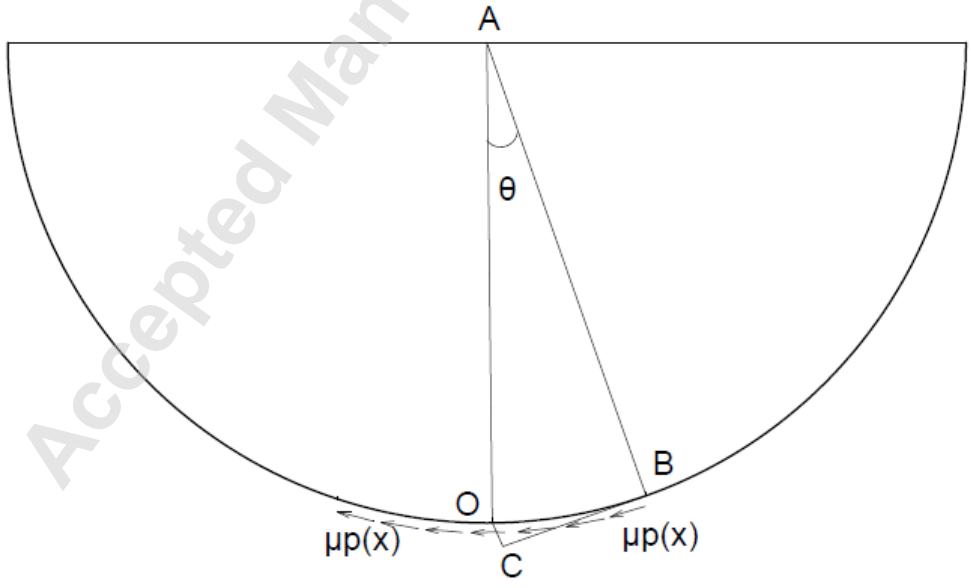

Figure 18: The schematic of the loading condition for estimation of the moment on the tip of the *half*-cylinder, M_0/L.

Journal of Applied Mechanics. Received January 08, 2019;
Accepted manuscript posted February 28, 2019. doi:10.1115/1.4043074

The tangential displacement of the stick region, δ_{i2}, can be estimated by assuming the block to be a half elastic space, and applying the Hertzian tangential traction, q(x), to the surface. At the initiation of gross slip, the local tangential traction in the contact region approaches q(x)=μp(x) within the contact region, [-b, b] (see Fig.2), and it is given by

$$q(x) = \mu p_0 \sqrt{1-\frac{x^2}{b^2}} \quad -b \le x \le b \tag{A15}$$

According to Johnson [9], for a half elastic space, the derivative of the displacement on the surface of a half elastic space is determined by the distributed tangential traction.

$$\int_{-b}^{b} \frac{\mu p_0}{b} \frac{\sqrt{b^2-s^2}}{x-s} ds = -\frac{\pi E}{2(1-\nu^2)} \frac{du}{dx} \tag{A16}$$

The integrations of left hand side of Eq. A16 are distinct for the regions inside and outside the contact region, thus

$$\frac{du}{dx} = \begin{Bmatrix} -\frac{2(1-\nu^2)\mu p_0}{bE}(x+\sqrt{x^2-b^2}) & (-\infty,-b) \\ -\frac{2(1-\nu^2)\mu p_0}{bE} x & (-b,b) \\ -\frac{2(1-\nu^2)\mu p_0}{bE}(x-\sqrt{x^2-b^2}) & (b,+\infty) \end{Bmatrix} \tag{A17}$$

Consequently, the tangential displacement on the surface, u, can be obtained by integrating Eq. A17. Here, we take the initial center of the contact as the datum, i.e., u(0)=0. Then u(x) can be derived to give:

$$u = \begin{Bmatrix} -\frac{(1-\nu^2)\mu p_0}{bE}(x^2 + x\sqrt{x^2-b^2} - b^2 \ln\frac{-x-\sqrt{x^2-b^2}}{b}) & (-\infty,-b) \\ -\frac{(1-\nu^2)\mu p_0}{bE} x^2 & (-b,b) \\ -\frac{(1-\nu^2)\mu p_0}{bE}(x^2 - x\sqrt{x^2-b^2} + b^2 \ln\frac{x+\sqrt{x^2-b^2}}{b}) & (b,+\infty) \end{Bmatrix} \tag{A18}$$

Journal of Applied Mechanics. Received January 08, 2019;
Accepted manuscript posted February 28, 2019. doi:10.1115/1.4043074

Note the similitude of Eq. A18 for (-b, b) and Eq. 15. The displacement of the stick region, δ_{i2}, at initiation of gross slip can be estimated by taking the difference between the u(x) at the leftmost position (x=-2R) and the center of the contact (x=0). Thus, the estimation of δ_{i2} is, δ_{i2}=u (0)-u (-2R), giving:

$$\delta_{i2} = \frac{(1-\nu^2)\mu p_0}{bE}(4R^2 - 2R\sqrt{4R^2-b^2} - b^2 \ln\frac{2R-\sqrt{4R^2-b^2}}{b}) \quad \text{(A19)}$$

If the contact width is much smaller than the radius, b<<R, Eq. A19 can be approximated while also using Eq. 2 for p_0 to finally result in:

$$\delta_{i2} = \frac{(1-\nu^2)\mu P}{\pi EL}(1-2\ln\frac{b}{4R}) \quad \text{(A20)}$$

This result shows a linear relation with respect to μ, and a nearly linear with respect to P/L (the nonlinearity is caused by the term ln (b/4R), where by Eq. 3, b is a function of P/L).

Reference

[1] Vingsbo, O., and Söderberg, S., 1988, "On fretting maps," Wear, 126(2), pp. 131-147.
[2] Varenberg, M., Etsion, I., and Halperin, G., 2004, "Slip Index: A New Unified Approach to Fretting," Tribology Letters, 17(3), pp. 569-573.
[3] Tabor, D., 1959, "Junction growth in metallic friction: the role of combined stresses and surface contamination," Proceedings of the Royal Society of London A: Mathematical, Physical and Engineering Sciences, 251(1266), pp. 378-393.
[4] Parker, R., and Hatch, D., 1950, "The static coefficient of friction and the area of contact," Proceedings of the Physical Society. Section B, 63(3), p. 185.
[5] McColl, I., Ding, J., and Leen, S., 2004, "Finite element simulation and experimental validation of fretting wear," Wear, 256(11-12), pp. 1114-1127.
[6] Kim, D.-G., and Lee, Y.-Z., 2001, "Experimental investigation on sliding and fretting wear of steam generator tube materials," Wear, 250(1-12), pp. 673-680.
[7] Zhu, M., Zhou, Z., Kapsa, P., and Vincent, L., 2001, "An experimental investigation on composite fretting mode," Tribology International, 34(11), pp. 733-738.
[8] Ahmadi, A., Sadeghi, F., and Shaffer, S., 2018, "In-Situ Friction and Fretting Wear Measurements of Inconel 617 at Elevated Temperatures," Wear, 410-411, pp. 110-118.
[9] Johnson, K. L., 1987, Contact mechanics, Cambridge university press.
[10] Popov, V. L., and Heß, M., 2015, Method of dimensionality reduction in contact mechanics and friction, Springer.
[11] Kogut, L. E., I, 2002, "Elastic–plastic contact analysis of a sphere and a rigid flat," ASME J. Appl. Mech, 69(5), pp. 657-662.

[12] Jackson, R. L., and Green, I., 2005, "A finite element study of elasto-plastic hemispherical contact against a rigid flat," Transactions of the ASME-F-Journal of Tribology, 127(2), pp. 343-354.
[13] Tsukizoe, T., and Hisakado, T., 1968, "On the Mechanism of Contact Between Metal Surfaces: Part 2—The Real Area and the Number of the Contact Points," Journal of Lubrication Technology, 90(1), pp. 81-88.
[14] Green, I., 2005, "Poisson ratio effects and critical valus in spherical and cylindrical Hertzian contacts," Applied Mechanics and Engineering, 10(3), p. 451.
[15] Gupta, V., Bastias, P., Hahn, G. T., and Rubin, C. A., 1993, "Elasto-plastic finite-element analysis of 2-D rolling-plus-sliding contact with temperature-dependent bearing steel material properties," Wear, 169(2), pp. 251-256.
[16] Yang, H., and Green, I., 2018, "A fretting finite element investigation of a plane-strain cylindrical contact of Inconel 617/ Incoloy 800H at room and high temperature," Pro IMechE Part J: J Engineering Tribology, pp. 1-17.
[17] Yang, H., and Green, I., 2018, "An Elasto-plastic finite element study of displacement-controlled fretting in a plane-strain cylindrical contact," ASME Trans., Journal of Tribology, 041401-1-041401-11.
[18] Yang, H., and Green, I., 2019, "Analysis of Displacement-Controlled Fretting Between a Hemisphere and a Flat Block in Elasto-Plastic Contacts," Journal of Tribology, 141(3), p. 031401.
[19] Ghosh, A., Leonard, B., and Sadeghi, F., 2013, "A stress based damage mechanics model to simulate fretting wear of Hertzian line contact in partial slip," Wear, 307(1), pp. 87-99.
[20] Archard, J., and Hirst, W., 1956, "The wear of metals under unlubricated conditions," Proc. R. Soc. Lond. A, 236(1206), pp. 397-410.
[21] METALS, S., 2008, "PRODUCT HANDBOOK OF HIGHPERFORMANCE NICKEL ALLOYS,"Product Handbook.
[22] ANSYS®SAS IP, I., Release 17.0, Help System, Mechanical APDL Contact Technology Guide, ANSYS, Inc.
[23] Timoshenko, S. P., 1921, "On the correction for shear of the differential equation for transverse vibrations of prismatic bars," The London, Edinburgh, and Dublin Philosophical Magazine and Journal of Science, 41(245), pp. 744-746.
[24] Cowper, G., 1966, "The shear coefficient in Timoshenko's beam theory," Journal of applied mechanics, 33(2), pp. 335-340.